Colloid Polym Sci 275:18–37 (1997)

ORIGINAL CONTRIBUTION

I.G. Voigt-Martin
Z.X. Zhang
D.H. Yan
A. Yakimanski
R. Matschiner
P. Krämer
C. Glania
D. Schollmeyer
R. Wortmann
N. Detzer

Structural dependence of non-linear optical properties of 4-Dimethylamino-3-cyanobiphenyl

Received: 15 April 1996
Accepted: 21 June 1996

Dr. I.G. Voigt-Martin (✉) · Z.X. Zhang
D.H. Yan · A. Yakimanski · R. Matschiner
Dr. P. Krämer · Dr. C. Glania
Dr. R. Wortmann · Dr. N. Detzer
Institut für Physikalische Chemie
der Universität Mainz
Jakob Welder Weg 11
55099 Mainz, FRG

Dr. D. Schollmeyer
Institut für Organische Chemie
der Universität Mainz
Jakob Welder Weg 11
55099 Mainz, FRG

Abstract 4-Dimethylamino-3-cyanobiphenyl (4-DMA-3-CB) was characterized with respect to linear and nonlinear optical properties in a crystal as well as in solution. The crystal structure was studied dependent on the crystallization conditions. It is shown that the crystal structure exhibiting NLO-activity can completely be solved by a combination of electron diffraction and computer modeling. There are four molecules per unit cell in the space group $Pna2_1$ with dimensions $a = 10.28$ Å, $b = 22.64$ Å, $c = 5.27$ Å. From this model structure the values and orientation of the dipole μ and static second order polarizability β can be calculated. Their relevance to the values obtained by a combination of polarization dependent measurements of Electric Field Induced Second Harmonic Generation (EFISH) and Hyper-Rayleigh-Scattering (HRS) in solution are discussed. The molecular second order polarizability tensor was found to be dominated by one single component. The orientations of the dipole and the vectorial parts of the second order polarizability delivered by the semiempirical calculations are in good agreement with the results of the EFISH and HRS-measurements and allow a deeper insight into the nonlinear optical properties of the crystal.

Key words Non-linear optics – electron diffraction

Introduction

A major aim in organic materials science is to design molecular architecture so as to fulfill specific criteria with regard to their physical properties in the condensed phase. In order to achieve this, it is necessary to know the molecular conformation and packing in the crystalline phase. Due to the availability of powerful computer technology, it is now possible to solve the crystal structure from electron diffraction data in those cases where crystals are too small for x-ray analysis and to compare the molecular conformation in the crystal field with that of the free molecule obtained experimentally and by semi-empirical quantum mechanical calculations.

In this paper it is shown how information about charge distribution in molecules, as well as the directions and values of dipoles and second order polarizabilities, can be obtained from a combination of electron diffraction and computer modeling. From this information the relationship between the macroscopic optical susceptibility and molecular second order polarizability parameters of a newly synthesized molecule is clarified. It is demonstrated that the structure of large crystals suitable for x-ray crystallography is different.

The molecule chosen for these investigations is 4-Dimethylamino-3-cyanobiphenyl (4-DMA-3-CB). Its molecular geometry with chemical formula $C_{15}H_{14}N_2$ is shown in the schematic diagram below (Fig. 1). It is apparent that the individual molecule is non-centrosymmetric

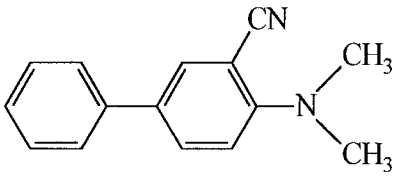

Fig. 1 Molecular geometry of 4-DMA-3-CB

and that the positions of the donating $N(CH_3)_2$ group and the acceptor (CN) should give rise to a dipole in a direction almost perpendicular to the long molecular axis.

For the characterization of the molecular second order polarizability tensor $\beta(-2\omega;\omega,\omega)$ of such a nonsymmetric molecule, one single method is not sufficient. Therefore, we use a combination of polarization dependent EFISH and HRS-measurements in order to obtain a maximum of information necessary for the comparison with the results of the semiempirical calculations and crystal properties. The molecule was not designed in order to get a maximized β, but to study the NLO-properties from different points of view. For β we use the Taylor-series definition as defined in ref. [1].

Theoretical background

Hyper Rayleigh Scattering (HRS)

The Hyper-Rayleigh-Scattering technique [2] has been developed by Clays and Persoons [3, 4] as a method for the determination of molecular second order polarizabilities. Collecting the frequency doubled light scattered perpendicular to the propagation direction of an intense laser beam in an isotropic liquid, one obtains information about the second order polarizability of the solute as described by various authors [3–5]. Measurements of the scattered intensity obtained by varying the mass fraction of the solute in the solvent yield the partial molar quantity (PMQ) P_2^*, which can be converted to the corresponding model-molar-quantity (MMQ) π_2^* applying the general formalism given by Liptay [7, 8] (starred quantities refer to the limit of vanishing mass fraction of the solute). This correction accounts for the concentration dependence of the local field factors. When carrying out the experiment with different polarization conditions of the fundamental laser and the collected scattered light it is possible to determine in principal five independent terms containing products of beta-components [9–11]. With Y being the propagation direction of the fundamental laser beam in the laboratory fixed frame (upper case indices), one obtains for linearly (Z) and circularly (C) polarized light and detection in Z and X-direction four different MMQ's. Their microscopic interpretation is given by

$$\pi^*_{2RS} = N_A (f^{2\omega})^2 (f^{\omega})^4 \langle \beta^2 \rangle_{RS} , \tag{1}$$

with R, S = C, Z or X. f^{ω} and $f^{2\omega}$ are appropriate local field factors. A discussion of the different models for the local fields is given in ref. 6.

The evaluation of the $\langle \beta^2 \rangle_{RS}$ has been given for various symmetry groups like C_{2v}, D_{3h} or C_{4v} in the literature [5, 6, 10–12]. Taking into account only the intrinsic permutation-symmetry of the β-tensor in the last two indices and by using standard methods of orientational averaging [13], we obtained as general expressions for molecules with C_1-symmetry:

$$\begin{aligned}
\langle \beta^2 \rangle_{ZZ} = \frac{1}{210} \cdot (&30\beta^2_{xxx} + 24\beta^2_{xyx} + 12\beta_{xxx}\beta_{xyy} + 6\beta^2_{xyy} + 24\beta^2_{xzx} \\
&+ 8\beta^2_{xzy} + 12\beta_{xxx}\beta_{xzz} + 4\beta_{xyy}\beta_{xzz} + 6\beta^2_{xzz} \\
&+ 24\beta_{xyx}\beta_{yxx} + 6\beta^2_{yxx} + 24\beta_{xxx}\beta_{yyx} + 24\beta_{xyy}\beta_{yyx} \\
&+ 8\beta_{xzz}\beta_{yyx} + 24\beta^2_{yyx} + 24\beta_{xyx}\beta_{yyy} + 12\beta_{yxx}\beta_{yyy} \\
&+ 30\beta^2_{yyy} + 16\beta_{xzy}\beta_{yzx} + 8\beta^2_{yzx} + 16\beta_{xzx}\beta_{yzy} + 24\beta^2_{yzy} \\
&+ 8\beta_{xyx}\beta_{yzz} + 4\beta_{yxx}\beta_{yzz} + 12\beta_{yyy}\beta_{yzz} + 6\beta^2_{yzz} \\
&+ 24\beta_{xzx}\beta_{zxx} + 8\beta_{yzy}\beta_{zxx} + 6\beta^2_{zxx} + 16\beta_{xzy}\beta_{zyx} \\
&+ 16\beta_{yzx}\beta_{zyx} + 8\beta^2_{zyx} + 8\beta_{xzx}\beta_{zyy} + 24\beta_{yzy}\beta_{zyy} \\
&+ 4\beta_{zxx}\beta_{zyy} + 6\beta^2_{zyy} + 24\beta_{xxx}\beta_{zzx} + 8\beta_{xyy}\beta_{zzx} \\
&+ 24\beta_{xzz}\beta_{zzx} + 16\beta_{yyx}\beta_{zzx} + 24\beta^2_{zzx} + 16\beta_{xyx}\beta_{zzy} \\
&+ 8\beta_{yxx}\beta_{zzy} + 24\beta_{yyy}\beta_{zzy} + 24\beta_{yzz}\beta_{zzy} \\
&+ 24\beta^2_{zzy} + 24\beta_{xzx}\beta_{zzz} + 24\beta_{yzy}\beta_{zzz} + 12\beta_{zxx}\beta_{zzz} \\
&+ 12\beta_{zyy}\beta_{zzz} + 30\beta^2_{zzz}) ,
\end{aligned} \tag{2}$$

$$\begin{aligned}
\langle \beta^2 \rangle_{ZX} = \frac{1}{210} \cdot (&6\beta^2_{xxx} + 16\beta^2_{xyx} + 8\beta_{xxx}\beta_{xyy} + 18\beta^2_{xyy} + 16\beta^2_{xzx} \\
&+ 24\beta^2_{xzy} + 8\beta_{xxx}\beta_{xzz} + 12\beta_{xyy}\beta_{xzz} + 18\beta^2_{xzz} \\
&- 12\beta_{xyx}\beta_{yxx} + 18\beta^2_{yxx} - 12\beta_{xxx}\beta_{yyx} - 12\beta_{xyy}\beta_{yyx} \\
&- 4\beta_{xzz}\beta_{yyx} + 16\beta^2_{yyx} - 12\beta_{xyx}\beta_{yyy} + 8\beta_{yxx}\beta_{yyy} \\
&+ 6\beta^2_{yyy} - 8\beta_{xzy}\beta_{yzx} + 24\beta^2_{yzx} - 8\beta_{xzx}\beta_{yzy} + 16\beta^2_{yzy} \\
&- 4\beta_{xyx}\beta_{yzz} + 12\beta_{yxx}\beta_{yzz} + 8\beta_{yyy}\beta_{yzz} + 18\beta^2_{yzz} \\
&- 12\beta_{xzx}\beta_{zxx} - 4\beta_{yzy}\beta_{zxx} + 18\beta^2_{zxx} - 8\beta_{xzy}\beta_{zyx} \\
&- 8\beta_{yzx}\beta_{zyx} + 24\beta^2_{zyx} - 4\beta_{xzx}\beta_{zyy} - 12\beta_{yzy}\beta_{zyy} \\
&+ 12\beta_{zxx}\beta_{zyy} + 18\beta^2_{zyy} - 12\beta_{xxx}\beta_{zzx} - 4\beta_{xyy}\beta_{zzx} \\
&- 12\beta_{xzz}\beta_{zzx} - 8\beta_{yyx}\beta_{zzx} + 16\beta^2_{zzx} - 8\beta_{xyx}\beta_{zzy}
\end{aligned}$$

$$-4\beta_{yxx}\beta_{zzy}-12\beta_{yyy}\beta_{zzy}-12\beta_{yzz}\beta_{zzy}+16\beta_{zzy}^2$$
$$-12\beta_{xzx}\beta_{zzz}-12\beta_{yzy}\beta_{zzz}+8\beta_{zxx}\beta_{zzz}$$
$$+8\beta_{zyy}\beta_{zzz}+6\beta_{zzz}^2)\,, \qquad (3)$$

$$\langle\beta^2\rangle_{CZ}=\frac{1}{210}\cdot(12\beta_{xxx}^2+32\beta_{xyx}^2-12\beta_{xxx}\beta_{xyy}+8\beta_{xyy}^2+32\beta_{xzx}^2$$
$$+20\beta_{xzy}^2-12\beta_{xxx}\beta_{xzz}-4\beta_{xyy}\beta_{xzz}+8\beta_{xzz}^2$$
$$+4\beta_{xyx}\beta_{yxx}+8\beta_{yxx}^2+4\beta_{xxx}\beta_{yyx}+4\beta_{xyy}\beta_{yyx}$$
$$-8\beta_{xzz}\beta_{yyx}+32\beta_{yyx}^2+4\beta_{xyx}\beta_{yyy}-12\beta_{yxx}\beta_{yyy}$$
$$+12\beta_{yyy}^2+12\beta_{xzy}\beta_{yzx}+20\beta_{yzx}^2+12\beta_{xzx}\beta_{yzy}$$
$$+32\beta_{yzy}^2-8\beta_{xyx}\beta_{yzz}-4\beta_{yxx}\beta_{yzz}-12\beta_{yyy}\beta_{yzz}$$
$$+8\beta_{yzz}^2+4\beta_{xzx}\beta_{zxx}-8\beta_{yzy}\beta_{zxx}+8\beta_{zxx}^2$$
$$+12\beta_{xzy}\beta_{zyx}+12\beta_{yzx}\beta_{zyx}+20\beta_{zyx}^2-8\beta_{xzx}\beta_{zyy}$$
$$+4\beta_{yzy}\beta_{zyy}-4\beta_{zxx}\beta_{zyy}+8\beta_{zyy}^2+4\beta_{xxx}\beta_{zzx}$$
$$-8\beta_{xyy}\beta_{zzx}+4\beta_{xzz}\beta_{zzx}+12\beta_{yyx}\beta_{zzx}$$
$$+32\beta_{zzx}^2+12\beta_{xyx}\beta_{zzy}-8\beta_{yxx}\beta_{zzy}+4\beta_{yyy}\beta_{zzy}$$
$$+4\beta_{yzz}\beta_{zzy}+32\beta_{zzy}^2+4\beta_{xzx}\beta_{zzz}+4\beta_{yzy}\beta_{zzz}$$
$$-12\beta_{zxx}\beta_{zzz}-12\beta_{zyy}\beta_{zzz}+12\beta_{zzz}^2)\,, \qquad (4)$$

$$\langle\beta^2\rangle_{CX}=\frac{1}{210}\cdot(4\beta_{xxx}^2+20\beta_{xyx}^2-4\beta_{xxx}\beta_{xyy}+12\beta_{xyy}^2+20\beta_{xzx}^2$$
$$+44\beta_{xzy}^2-4\beta_{xxx}\beta_{xzz}-20\beta_{xyy}\beta_{xzz}+12\beta_{xzz}^2$$
$$-8\beta_{xyx}\beta_{yxx}+12\beta_{yxx}^2-8\beta_{xxx}\beta_{yyx}-8\beta_{xyy}\beta_{yyx}$$
$$+16\beta_{xzz}\beta_{yyx}+20\beta_{yyx}^2-8\beta_{xyx}\beta_{yyy}-4\beta_{yxx}\beta_{yyy}$$
$$+4\beta_{yyy}^2-24\beta_{xzy}\beta_{yzx}+44\beta_{yzx}^2-24\beta_{xzx}\beta_{yzy}$$
$$+20\beta_{yzy}^2+16\beta_{xyx}\beta_{yzz}-20\beta_{yxx}\beta_{yzz}-4\beta_{yyy}\beta_{yzz}$$
$$+12\beta_{yzz}^2-8\beta_{xzx}\beta_{zxx}+16\beta_{yzy}\beta_{zxx}+12\beta_{zxx}^2$$
$$-24\beta_{xzy}\beta_{zyx}-24\beta_{yzx}\beta_{zyx}+44\beta_{zyx}^2+16\beta_{xzx}\beta_{zyy}$$
$$-8\beta_{yzy}\beta_{zyy}-20\beta_{zxx}\beta_{zyy}+12\beta_{zyy}^2-8\beta_{xxx}\beta_{zzx}$$
$$+16\beta_{xyy}\beta_{zzx}-8\beta_{xzz}\beta_{zzx}-24\beta_{yyx}\beta_{zzx}$$
$$+20\beta_{zzx}^2-24\beta_{xyx}\beta_{zzy}+16\beta_{yxx}\beta_{zzy}-8\beta_{yyy}\beta_{zzy}$$
$$-8\beta_{yzz}\beta_{zzy}+20\beta_{zzy}^2-8\beta_{xzx}\beta_{zzz}-8\beta_{yzy}\beta_{zzz}$$
$$-4\beta_{zxx}\beta_{zzz}-4\beta_{zyy}\beta_{zzz}+4\beta_{zzz}^2)\,. \qquad (5)$$

If only one β-component is significant the molecular fixed frame (lower case indices) may be chosen in such a way that this component is β_{xxx} or β_{yyy} or β_{zzz}. In this case one obtains for the depolarization ratios

$$\rho_{ZX}^{ZZ}=\pi_{2ZZ}^*/\pi_{2ZX}^*=5.0\,, \qquad (6)$$

$$\rho_{CX}^{CZ}=\pi_{2CZ}^*/\pi_{2CX}^*=3.0\,, \qquad (7)$$

$$\rho_{ZX}^{CZ}=\pi_{2CZ}^*/\pi_{2ZX}^*=2.0\,. \qquad (8)$$

Deviations from these depolarization ratios indicate the significance of more than one tensor component. Equation (8) is also valid if the β-tensor has more than one significant component but is symmetrical by permutation over all indices (Kleinman's symmetry), as pointed out by Heesink et al. [9].

Electric Field Induced Second Harmonic Generation (EFISH)

The EFISH-technique [14] utilizes an external static electric field $\mathbf{E}_0$ to induce an effective second-order susceptibility

$$\boldsymbol{\chi}^{(2)}(-2\omega;\omega,\omega;E^0)=3\cdot\boldsymbol{\chi}^{(3)}(-2\omega;\omega,\omega,0)\cdot\mathbf{E}^0 \qquad (9)$$

in a liquid solution. In general, $\chi^{(2)}(-2\omega;\omega,\omega;E^0)$ is measured by a wedge fringe method. For theoretical and experimental details see ref. [15].

A symmetry consideration shows that the third-order nonlinearity $\chi^{(3)}(-2\omega;\omega,\omega,0)$ of a medium which is isotropic in the absence of any externally applied electric field has only two independent components, $\chi_{ZZZZ}^{(3)}$ and $\chi_{ZXXZ}^{(3)}$. In the first case the electric field vector of the fundamental laser beam is parallel, in the latter perpendicular to the external electric field E_0.

The evaluation of concentration dependent EFISH-measurement yields the partial molar third-order polarizabilities

$$\mathbf{Z}_2^{(3)*}(-2\omega;\omega,\omega,0)$$
$$=\lim_{n_2\to 0}\left(\frac{\partial[\varepsilon_0\chi^{(3)}(-2\omega;\omega,\omega,0)V]}{\partial n_2}\right)_{p,T,n_1}\,, \qquad (10)$$

with the pressure p and the volume V of the phase and the amounts of the solvent n_1 and the solute n_2. These PMQ's again can be converted to the corresponding MMQ's $\zeta_2^{(3)*}(-2\omega;\omega,\omega,0)$ by applying the general formalism given by Liptay [7, 8], in order to take into account the concentration dependence of the local fields. It necessitates knowledge of the influences of the solute on the density, refraction index and permittivity of the solution, which are expressed in terms of the corresponding partial molar quantities.

The microscopic interpretation of the MMQ's $\zeta_2^{(3)*}$ yields to the following expressions (the usually small contributions of the third order polarizability $\gamma(-2\omega;\omega,\omega,0)$ are neglected):

$$\zeta^{(3)*}_{2ZXXZ}(-2\omega;\omega,\omega,0) = \frac{1}{90} N_A f^0 (f^\omega)^2 f^{2\omega} \left[\frac{1}{kT}\boldsymbol{\mu}\cdot(2^1\boldsymbol{\beta} - {}^2\boldsymbol{\beta})\right], \quad (11)$$

$$\zeta^{(3)*}_{2ZZZZ}(-2\omega;\omega,\omega,0) = \frac{1}{90} N_A f^0 (f^\omega)^2 f^{2\omega} \left[\frac{1}{kT}\boldsymbol{\mu}\cdot(2^2\boldsymbol{\beta} + {}^1\boldsymbol{\beta})\right], \quad (12)$$

where N_A is Avogadro's number. For the local field factors see again the discussion in ref. [6].

The vector parts ${}^1\beta$ and ${}^2\beta$ of the second order polarizability tensor are given by (summation over repeated indices, indices in brackets are symmetric by permutation)

$${}^1\beta_r = \beta_{r(ss)}; \qquad {}^2\beta_r = \beta_{s(rs)} = \beta_{s(sr)}, \quad (13)$$

μ is the ground state dipole and can be obtained from the concentration dependence of the permittivity. This leads to the corresponding PMQ $Z_2^{(1)*}(0;0)$ and MMQ $\zeta_2^{(1)}(0;0)$. Details of the evaluation are given in ref. [8].

In case of Kleinman's symmetry (permutation symmetry in all indices), the two vector parts of the second order polarizability are identical:

$${}^1\beta_r = {}^2\beta_r = {}^v\beta_r . \quad (14)$$

This yields the following expression for the EFISH-MMQ's:

$$\zeta^{(3)*}_{2ZZZZ} = 3\zeta^{(3)*}_{2ZXXZ} = \frac{1}{30} N_A f^0 (f^\omega)^2 f^{2\omega} \left(\frac{1}{kT}\boldsymbol{\mu}\cdot{}^v\boldsymbol{\beta}\right). \quad (15)$$

With the ground state dipole obtained from permittivity measurements one can evaluate the vector parts of the second order polarizability according to Eqs. (11, 12) in general or Eq. (15) in the special case of Kleinman's symmetry being valid.

Second harmonic generation in crystals (SHG)

Both the dipole and second order polarizability depend on the molecular conformation, which is affected by the crystal field. The relevant information can be obtained from a combination of electron diffraction data with semi-empirical quantum mechanical calculations, as will be shown subsequently.

The relationship between macroscopic susceptibility χ_{IJK} in crystallographic axes (IJK) and the second order polarizability β_{ijk} in molecular axes is given by Eq. (16)

$$\chi_{IJK}(-\omega;\omega_1,\omega_2) = \frac{1}{V} f_I(\omega) f_J(\omega_1) f_K(\omega_2) \times \sum_{ijk} \cos\theta_{Ii}^{(s)} \cos\theta_{Jj}^{(s)} \cos\theta_{Kk}^{(s)} \beta_{ijk}(-\omega;\omega_1,\omega_2) \quad (16)$$

where V is the volume of the unit cell. $s = 1, 2 \ldots N_g$ indicates labeling of equivalent positions in the unit cell. θ_{Ii} = angle between crystallographic axis I and molecular axis i. f is a field factor.

χ and β are third rank tensors with 27 independent components. Depending on crystal symmetry (space group), the number of independent moduli is reduced, and for crystal classes with a center of symmetry all moduli vanish [16].

For this reason the space group of the crystal must be established by an appropriate diffraction experiment.

Calculation of molecular conformation

It will be shown in the following section that electron diffraction analysis delivers lower resolution information than x-ray diffraction for fundamental reasons. Therefore the minimum energy conformation calculated by semi-empirical quantum mechanical methods which is closest to the one obtained from the diffraction calculation is chosen for further discussion. Because the crystal field causes adjustments in molecular conformation, it is not necessary to invoke **ab initio** calculations; instead the semi-empirical AM1 and PM3 values calculated by MOPAC are sufficiently accurate to initialize the crystallography programs. Since second order polarizabilities are frequently defined using differing conventions, it must be noted that the semi-empirical calculations use the finite field technique [17]. These methods have been parametrized for gas phase properties such as ground state geometries, dipoles μ and heats of formation, but not for the second order polarizability β. Generally, the second order polarizability values obtained by these methods are intermediate between those obtained by self-consistent field (SCF) and second order perturbation (MP2) calculations.

When comparing the values of β with the results of the measurements, great care has to be taken: The finite field method incorporated in MOPAC gives values for the static second order polarizability $\beta(0;0,0)$. The optical values $\beta(-2\omega;\omega,\omega)$ obtained from the experiments are enhanced with respect to the static ones by dispersion and by the influence of the reaction field in solution [2, 6, 18]. In general the calculated values are therefore expected to be significantly lower than the experimentally obtained ones.

Structure determination by electron diffraction

Electron diffraction structure analysis must be used when crystals are too small for any other method. In the kinematic approximation, the distribution of scattering power in the lattice $|\mathbf{F(u)}|^2$ in electron diffraction experiments consists of a sharp peak around each reciprocal point of the form $|\mathbf{S(u)}|^2$ [19, 20]:

$$|\mathbf{F(u)}|^2 = \sum_h \sum_k \sum_l |\mathbf{F}_{hkl}|^2 \delta\{\mathbf{u} - (h\mathbf{a}^* + k\mathbf{b}^* + l\mathbf{c}^*)\} \cdot |\mathbf{S(u)}|^2 \tag{17}$$

and the inverse transformation gives a Patterson function indicating the potential distribution:

$$P(X, Y, Z) = V^{-1} \sum_h \sum_k \sum_l \exp\left\{-2\pi i\left(\frac{hx}{a} + \frac{ky}{b} + \frac{lz}{c}\right)\right\} \times [s(r) \cdot s(-r)] \,. \tag{18}$$

As in all diffraction experiments the phase information (i.e. about positions of atoms) is lost. These can only be calculated by **ab initio** methods such as direct phase [21] or maximum entropy [22] or by using simulation methods [23, 24].

For the experiments described here, we have chosen the simulation technique described in the experimental section.

The primary information about possible arrangements of atoms in the unit cell is contained in the symmetry of the crystal structure. As in x-ray diffraction, the space group can be obtained by studying systematic absences in the diffraction pattern from different projections. The principle difficulty lies in the fact that the electron intensities are affected by dynamical and secondary scattering to such an extent that characteristic extinctions may even be masked altogether [19, 20]. To recognize such effects, many different projections are required before the space group can be reliably assessed. We have shown previously how the space group determined experimentally can be related to the symmetry of the molecule determined by semi-empirical calculations. Successful packing in the unit cell with the correct symmetry can be achieved by re-optimizing the molecular conformation and thus reducing the packing energy until negative values are obtained [24, 25].

Experimental methods

HRS and EFISH in solution

The HRS-device was described in ref [6]. Linear and circular polarization of the fundamental laser beam (Nd:YAG, 1064 nm) were obtained by the use of appropriate quarter- and half wave plates. Depolarization ratios were determined by subsequent reduction of the detection aperture and extrapolating to zero space angle as described in ref [6]. The device was calibrated against pNA in dioxane. β_{zzz} for pNA was determined as $27.4 \cdot 10^{-50}$ Cm^3V^{-2} by EFISH-measurements. This has been proven to be the only significant tensor component [15]. This method of calibration is more accurate than the frequently suggested calibration against the solvent [6, 26].

The EFISH device was described in ref. [15]. It was calibrated against a quartz crystal with $d_{11} = 0.5$ pmV^{-1}.

Absorption spectra were recorded on a Perkin–Elmer UV/340 UV/vis/near-IR spectrometer using Suprasil quartz cells. Density measurements were made with a vibrating densimeter (DMA 02 Paar KG, Graz), refractometric measurements with a Pulfrich refractometer (Bellingham and Stanley) at $\lambda = 589$ nm, and permittivity measurements with a DM 01 dipole meter (WTW Weilheim).

Dioxane was purified by column chromatography (alumina basic, act. super 1, argon atmosphere), rectified and distilled from sodium/potassium alloy prior to use. Methylcyclohexane was purified by distillation followed by two chromatographic procedures: The stationary phase for the first chromatography was prepared by loading alumina (act. super I, 900 g) with conc. sulfuric acid (60 g) and conc. nitric acid (60 g) over 3 h using a rotary evaporator. For the second chromatography alumina basic act. super I was used. Finally, the methylcyclohexane was rectified and distilled from sodium/potassium alloy prior to use.

The purity of 4-DMA-3-CB was checked by elementary analysis, FD-MS and TLC. Details of the synthesis will be published later.

Optical measurements on crystals

Crystals were screened for SHG response by illuminating them with infrared light ($\lambda = 1064$ nm) using the fundamental beam of a Q-switched Nd:YLF laser. The incident beam (TEM beam diameter 0.9 mm, polarization 100:1) is focused via a beam-splitting mirror onto the sample placed on a microscope specimen stage [27]. The fundamental intensity in the plane of the crystal would be 10^8 W/cm^2, so that an infrared filter is positioned in front of the objective lens to protect the sample. If the sample generates a second harmonic signal, an additional bandpass filter ($\lambda = 532.5$ nm) guarantees that only this signal reaches the detector (or camera).

Sample preparation for structure analysis

Single crystals of 4-DMA-3CB were grown from solution in ethanol using both slow and fast crystallization rates. After slow crystallization, crystals large enough for x-ray structure analysis and refinement were obtained ($\sim 5\,\text{mm} * 2\,\text{mm} * 0.5\,\text{mm}$). The crystals obtained after rapid crystallization were too small for an x-ray structure determination ($\sim 10\,\mu\text{m} * 5\,\mu\text{m} * 10\,\text{nm}$) and were therefore investigated by electron diffraction.

Electron diffraction

The samples were placed on electron-microscope grids and investigated in a Philips 300 electron-microscope with a goniometer stage.

A rotation/tilt holder was used to obtain different crystallographic projections of the unit cell. The sample was rotated in the holder until a suitable crystallographic axis corresponded to the tilt axis. The tilt angle was then adjusted until new zones appeared until the maximum tilting angle of $\pm 60°$ was reached. Subsequently another axis is chosen and the procedure repeated. In this way a large region of reciprocal space can be scanned, excepting a cone containing atomic planes from 0°–30° to the crystal surface.

The theoretical concepts related to electron diffraction are well known [19, 20]. In practice the following points must be taken into account:

1) The measured intensities may be unreliable because the scattering process involves secondary, inelastic and dynamic effects [19, 20]. Experimentally this means that symmetry forbidden reflections may appear and intensities are modified.

2) In order to determine the space group and obtain 3-D data, a tilting series is essential but time consuming. During this procedure intensities may be changed as the sample is destroyed by the electron beam [23, 28–30].

3) Due to the limited linear range of the photographic emulsion, an exposure series must be obtained, thus increasing the risk that the intensities are changed during data collection due to beam exposure.

4) During a tilting experiment, the sample thickness traversed by the electron beam increases, thus altering the intensities in a non-linear manner due to dynamic and secondary scattering. For these reasons electron crystallography is not a standard technique which can be applied routinely.

Despite these difficulties, it is possible to derive the cell constants and a limited number of possible space groups based on the tilting series experiments. Simulation of experimental electron diffraction patterns in all zones using CERIUS then enables the molecular conformation to be derived and the appropriate molecular parameters to be calculated [23–25, 30–32]. Instead of simulations, direct methods of analysis may be applied successfully to solve the structure of many organic molecules; the state of the art has been reviewed by Dorset [33, 34]. Alternatively, statistical methods based on information theory have also been applied successfully to organic molecules [22, 32, 35, 36].

The many successful structure determinations including refinement based on electron diffraction data demonstrate that the methods all work under appropriate experimental conditions despite the fact that quantitative intensity values are acknowledged to be poor. For direct and maximum entropy methods, correct phase predictions are possible for reasons described in the quoted literature; in the case of the simulation method, model structures can be predicted because there are so many restrictions on a) possible molecular conformations due to covalent bond lengths, torsion angles, and symmetry b) possible crystallographic packing due to permissible Van der Waals distances, densities and permissible crystal symmetry.

The necessity of obtaining a negative packing energy strongly restricted the possible conformations. The procedure has been described in detail previously [24, 25, 31, 32].

Powder X-ray diffraction

X-ray powder diffraction patterns were obtained by standard methods using a Siemens D 500 diffractometer (Cu K_α radiation with a wavelength $\lambda = 1.542$ Å) in a $\theta/2\theta$ x-ray reflectivity mode. As is often found in organic samples, the number of reflections does not suffice for Rietveld methods. If the unit cell obtained from electron diffraction is correct, consistent indexing can be achieved and the cell parameter not available in the tilting experiment can be derived.

In addition, the appearance of forbidden reflections in the electron diffraction patterns can be tested.

X-ray structure analysis

The structure of those crystals obtained by slow crystallization and large enough for x-ray analysis was solved by direct methods using SHELX86 [37] and refined by full-matrix least square analysis using SHELX93 [38]. The data was reduced. Lorentz and polarization correction were applied using a local data reduction program. Non-H atoms were refined anisotropically, H atoms were placed

at geometrically calculated positions and refined with riding motion.

Computational methods

Generation of molecular model

The minimum energy gas phase conformations of the molecules were calculated by semi-empirical quantum mechanical methods incorporated in MOPAC. The method has been established in quantum chemistry for many years [39]. For optimization of parameters (such as heat of formation, dipoles, ionization potentials) the program MNDO-PM3 was used, which is incorporated in the program package MOPAC 6.0 [40]. Most molecules produce several minimum energy conformations. To begin the simulation, the conformation which can best be fitted into the experimentally determined unit cell is chosen.

Simulation of electron diffraction pattern

In order to proceed with simulation of the electron diffraction patterns, the experimentally determined unit cell and space group are required. The MOPAC calculated molecule is placed into the unit cell using the molecular modeling program CERIUS such that the required symmetry requirements based on the experimentally observed extinctions are satisfied. In addition to this, the density must be correct.

Initially, the packing energy is generally positive and a number of non-allowed close contacts are observed. These can be eliminated by adjusting the required parameters using both translation and rotations of suitable subunits. Subsequently, the crystal packing energy is again minimized until a negative value is obtained. Its value is determined by a superposition of various two body, three body and four body interactions:

$$E = E_{\mathrm{VdW}} + E_{\mathrm{Coul}} + E_{\mathrm{hb}} + E_{\mathrm{tor}} \tag{19}$$

a) The Van der Waals term is treated using the Lennard–Jones functional form.

b) The Ewald summation technique is used to calculate the coulomb energy [41].

c) The energy of the hydrogen bonds is calculated using a CHARM-like potential.

d) A Dreiding force-field is used for the calculation of subrotation interactions [42].

Negative packing energies can generally be found for several structures, but comparison with the experimental diffraction patterns from different zones often reduce them to a unique solution.

Results

HRS and EFISH measurements

The results of the HRS, EFISH, refractometric, density and permittivity measurements are presented in Tables 1 and 2 in comparison with the results of the PM3-calculations for the single molecule. We used the Lorentz model modified as described in ref. [6] to correct for local field effects. As sufficient information about the anisotropy of

Table 1 Results of permittivity(a), refractometric(b)-, density(c)-, EFISH(d)- and HRS(e)-measurements on 4-DMA-3-CB in methylcyclohexane. Statistical errors correspond to 95% confidence

M_2		$(10^{-3}\ \mathrm{kg\ mol^{-1}})$	222.29
$Z_2^{(1)*}(0;0)$	(a)	$(10^{-16}\ \mathrm{C\ m^2\ V^{-1}\ mol^{-1}})$	200 ± 10
$\zeta_2^{(1)*}(0;0)$	(a)	$(10^{-16}\ \mathrm{C\ m^2\ V^{-1}\ mol^{-1}})$	154 ± 7
$Z_2^{(1)*}(-\omega;\omega)$	(b)	$(10^{-16}\ \mathrm{C\ m^2\ V^{-1}\ mol^{-1}})$	30 ± 1
$\zeta_2^{(1)*}(-\omega;\omega)$	(b)	$(10^{-16}\ \mathrm{C\ m^2\ V^{-1}\ mol^{-1}})$	27 ± 1
V_2^*	(c)	$(10^{-6}\ \mathrm{m^3\ mol^{-1}})$	202 ± 5
$Z_{2ZZZZ}^{(3)*}(-2\omega;\omega,\omega,0)$	(d)	$(10^{-36}\ \mathrm{C\ m^4\ V^{-3}\ mol^{-1}})$	8.1 ± 1.0
$\zeta_{2ZZZZ}^{(3)*}(-2\omega;\omega,\omega,0)$	(d)	$(10^{-36}\ \mathrm{C\ m^4\ V^{-3}\ mol^{-1}})$	5.2 ± 1.0
$Z_{2ZXXZ}^{(3)*}(-2\omega;\omega,\omega,0)$	(d)	$(10^{-36}\ \mathrm{C\ m^4\ V^{-3}\ mol^{-1}})$	2.7 ± 0.3
$\zeta_{2ZXXZ}^{(3)*}(-2\omega;\omega,\omega,0)$	(d)	$(10^{-36}\ \mathrm{C\ m^4\ V^{-3}\ mol^{-1}})$	1.7 ± 0.3
$\frac{\zeta_{2ZZZZ}^{(3)*}(-2\omega;\omega,\omega,0)}{\zeta_{2ZXXZ}^{(3)*}(-2\omega;\omega,\omega,0)}$	(d)	–	3.1 ± 0.8
P_{2ZZ}^*	(e)	$(10^{-74}\ \mathrm{C^2\ m^6\ V^{-4}\ mol^{-1}})$	0.44 ± 0.03
π_{2ZZ}^*	(e)	$(10^{-74}\ \mathrm{C^2\ m^6\ V^{-4}\ mol^{-1}})$	0.44 ± 0.03
ρ_{ZX}^{ZZ}	(e)	–	5.2 ± 0.3
ρ_{CX}^{CZ}	(e)	–	2.6 ± 0.5
ρ_{ZX}^{CZ}	(e)	–	2.1 ± 0.2

Table 2 Comparison between calculated and experimental molecular properties of 4-DMA-3CB. Statistical errors correspond to 95% confidence. PM3 calculations are performed for the single molecule. See text for β-definitions. The conversion factors to the esu units are: μ(Debye) = $2.998 \cdot 10^{29}$ μ(Cm); $\beta(10^{-30}$ esu) = 0.3712 $\beta(10^{-50}$ Cm^3 V^{-2})

Dipole			
$\lvert\mu\rvert$	(a)	(10^{-30} C m)	13.9 ± 0.4
μ_x	(d)	(10^{-30} C m)	-5.42
μ_y	(d)	(10^{-30} C m)	13.31
μ_z	(d)	(10^{-30} C m)	-2.23
$\lvert\mu\rvert$	(d)	(10^{-30} C m)	14.54
value of β along dipole			
$(\mu \cdot {}^1\beta)/\lvert\mu\rvert$	(b)	(10^{-50} C m^3 V^{-2})	2.85 ± 0.41
$(\mu \cdot {}^2\beta)/\lvert\mu\rvert$	(b)	(10^{-50} C m^3 V^{-2})	2.91 ± 0.67
$(\mu \cdot {}^1\beta)/\lvert\mu\rvert$	(d) (e)	(10^{-50} C m^3 V^{-2})	-0.49
dominant tensor component			
$\beta^{(HRS)}$	(c)	(10^{-50} C m^3 V^{-2})	11.40 ± 0.40
β_{xxx}	(d), (f)	(10^{-50} C m^3 V^{-2})	1.46

a) from permittivity measurements
b) from EFISH-measurements
c) from HRS-measurements
d) from PM3-calculations, single molecule, conformation closest to crystal conformation
e) the value of the vector component of β along the dipole given by MOPAC is defined as $3/5\ (\mu \cdot {}^1\beta)/\mu$, [16]the value given here is corrected with respect to this and fits with our definition
f) dominant component from PM3-calculations
x corresponds to direction of molecular axis
y direction is perpendicular (in plane of paper Fig. 7)
z perpendicular to both

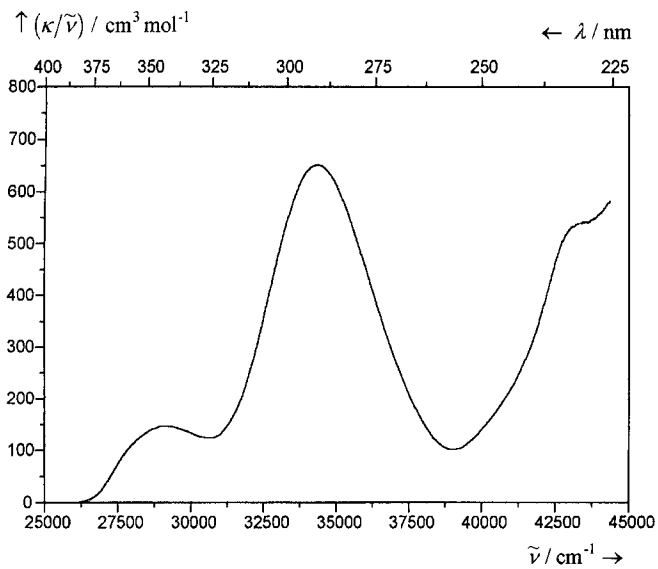

Fig. 2 Absorption spectrum of 4-DMA-3-CB in methylcyclohexane

the first order polarizability of 4-DMA-3CB is not available, the application of the ellipsoidal Onsager model was not possible.

An inspection of the results obtained for the depolarization ratios from HRS indicates that the second order

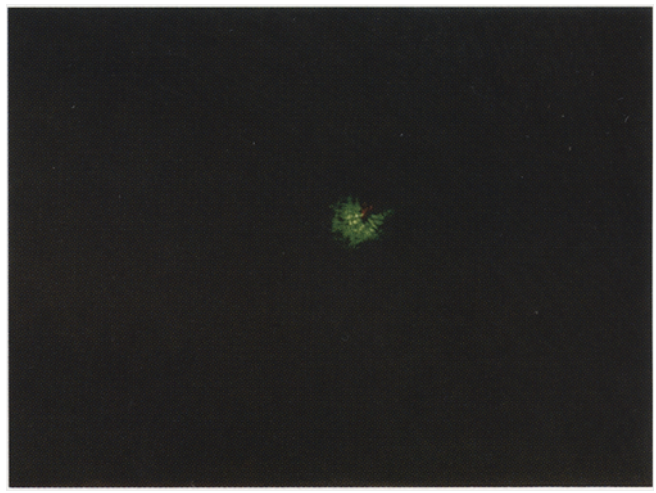

Fig. 3 SHG image of small DMA-3CB crystals

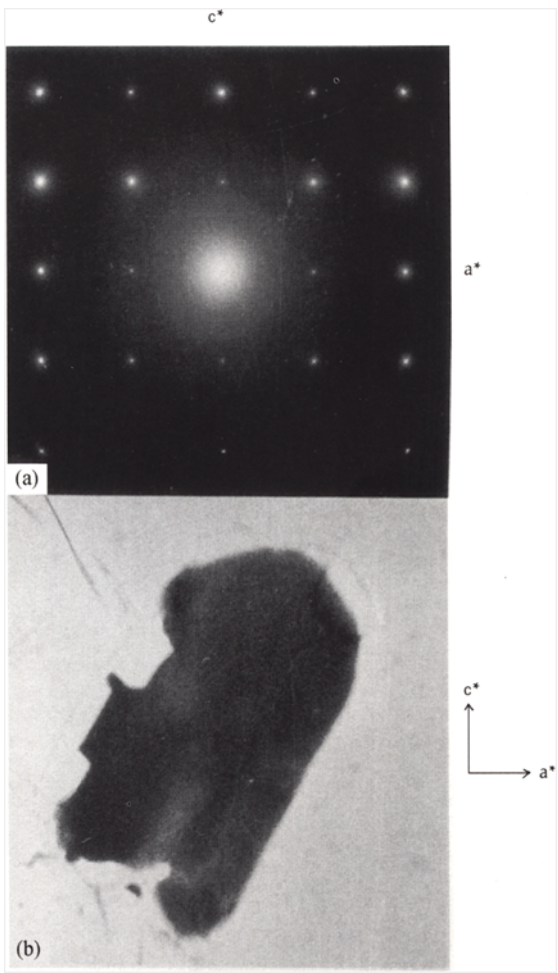

Fig. 4 Image and electron diffraction pattern of small DMA-3CB crystals

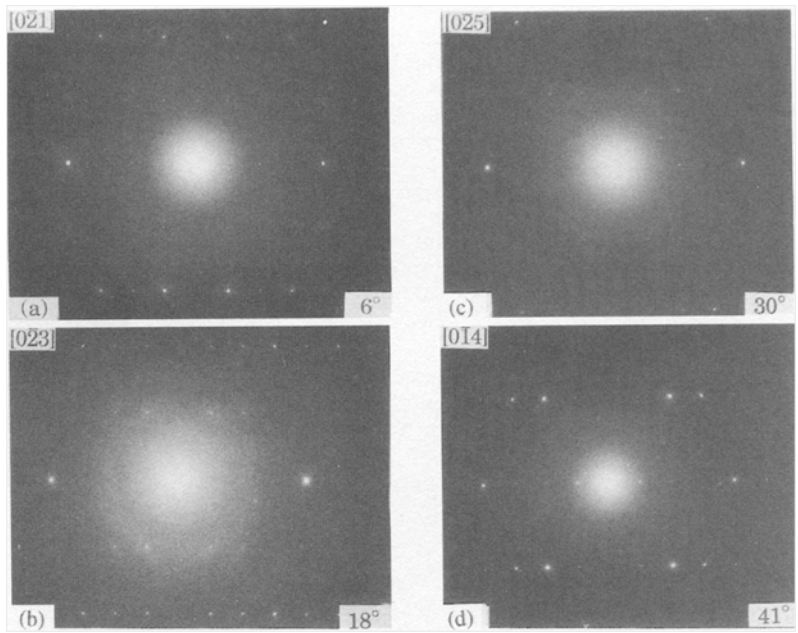

Fig. 5 Tilt series of DMA-3CB crystal about a* (Tilt angle indicated in lower right-hand corner and corresponding zone in upper left-hand corner)

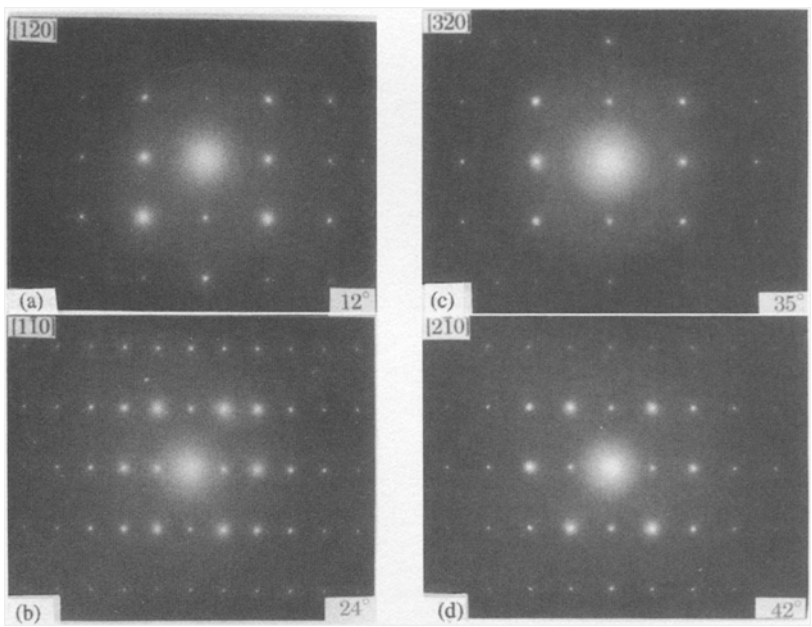

Fig. 6 Tilt series of DMA-3CB crystal about c* (Tilt angle indicated in lower right-hand corner and corresponding zone in upper left-hand corner)

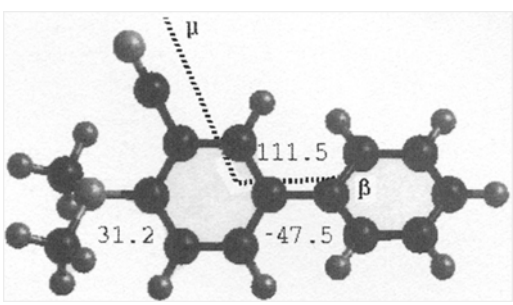

Fig. 7 MOPAC-calculated molecular conformation in the gas phase indicating direction of μ and β. 111.5 indicates angle between μ and β. The other angles are torsion angles with respect to central phenylene ring

Table 3 Calculated vector components of the second order polarizabilities β for a single molecule, closest to the conformation required in the crystal cell

Second order polarizability[a]		
$^1\beta_x$	(10^{-50} C m^3 V^{-2})	1.31
$^1\beta_y$	(10^{-50} C m^3 V^{-2})	0.17
$^1\beta_z$	(10^{-50} C m^3 V^{-2})	0.18
$\lvert^1\beta\rvert$	(10^{-50} C m^3 V^{-2})	1.33

[a] The definition of the vector parts in MOPAC differs by a factor of 3/5 from Eq. (13), the MOPAC value being lower. The values given here are corrected with respect to this and follow the definition in Eq. (13).

Table 4 Calculated dipole μ and second order polarizabilities β in crystal

Single molecule from space group $Pna2_1$		
Dipole		
μ_x	(10^{-30} C m)	−0.27
μ_y	(10^{-30} C m)	11.68
μ_z	(10^{-30} C m)	−0.84
$\lvert\mu\rvert$	(10^{-30} C m)	11.71
Second order polarizability[a]		
$^1\beta_x$	(10^{-50} C m^3 V^{-2})	5.39
$^1\beta_y$	(10^{-50} C m^3 V^{-2})	1.29
$^1\beta_z$	(10^{-50} C m^3 V^{-2})	−0.37
$\lvert^1\beta\rvert$	(10^{-50} C m^3 V^{-2})	5.56
$Pna2_1$ crystal (4 molecules/cell)		
Resultant dipole along crystal axis		
μ_a	(10^{-30} C m)	−0.26
μ_b	(10^{-30} C m)	1.69
μ_c	(10^{-30} C m)	38.95
$\lvert\mu\rvert$	(10^{-30} C m)	38.99
Resultant second order polarizability along crystal axis[a]		
$^1\beta_a$	(10^{-50} C m^3 V^{-2})	−0·07
$^1\beta_b$	(10^{-50} C m^3 V^{-2})	0.96
$^1\beta_c$	(10^{-50} C m^3 V^{-2})	4.22
$\lvert^1\beta\rvert$	(10^{-50} C m^3 V^{-2})	4.33

[a] Legend as in Table 3.

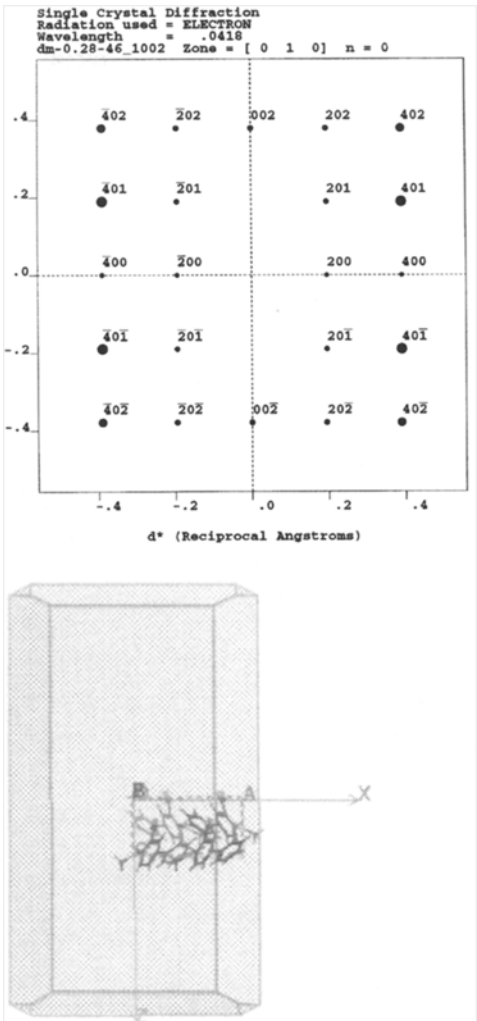

Fig. 8 Relationship between diffraction pattern and molecular orientation in unit cell with respect to macroscopic crystalline axes

polarizability tensor is dominated by one single component which is quite a surprising result for a molecule with C_1-symmetry. In order to avoid confusion with the definition of the molecular fixed frame used in Sec. $V(F)$ for the semi-empirical calculations, this single component is called $\beta^{(HRS)}$. The dominance of one single component trivially predicts the validity of Kleinman's symmetry, which is independently confirmed by the value of ρ_{ZX}^{CZ} [cf. Eq. (8)] from HRS and the value of $\xi^{(3)*}_{2zzzz}(-2\omega;\omega,\omega,0)/\xi^{(3)*}_{2zxxz}(-2\omega;\omega,\omega,0)$ [cf. Eq. (15)] from the EFISH-experiment. When comparing the absolute values for the second order polarizability it should be remembered that the information obtained by the two experiments is not identical: In the case of EFISH, one obtains the scalar product of the vector part defined in Eq. (13) with the ground state dipole, while HRS gives a linear combination of squares of all tensor components [cf. Eqs. (2–5)]. The fact that the result of the EFISH-experiment is much lower than the one of the HRS-experiment indicates that the vector part $^v\beta$ obtained by the EFISH-experiment is nearly perpendicular to the molecular ground state dipole. In such a case the absolute value for the dominant component $\beta^{(HRS)}$ can be obtained only by HRS.

The HRS-measurements were carried out in methylcyclohexane as well as in dioxane. The latter was done because the calibration standard pNA is not sufficiently solvable in methylcyclohexane. The value obtained for ρ_{ZX}^{ZZ} was equal within experimental errors, the value for $\beta^{(HRS)} = (13.1 \pm 0.8)\cdot 10^{-50}$ Cm^3 V^{-2} is slightly higher than the one in methylcyclohexane, which can be interpreted as an effect of the reaction field. When comparing the results for β with the value published for the 4,4′-isomer [43, 44] there are two striking differences. The absolute value for $\beta^{(HRS)}$ is significantly lower reflecting the less effective o-substitution with respect to the *p*-substitution. The second difference is that in 4-DMA-3CB the ground state dipole does not coincide with the vector part of β containing $\beta^{(HRS)}$, as is the case for 4,4′-isomer for reasons of molecular symmetry and topology. This gives rise to the interesting molecular and crystal properties of 4-DMA-3CB.

Colloid & Polymer Science, Vol. 275, No. 1 (1997)

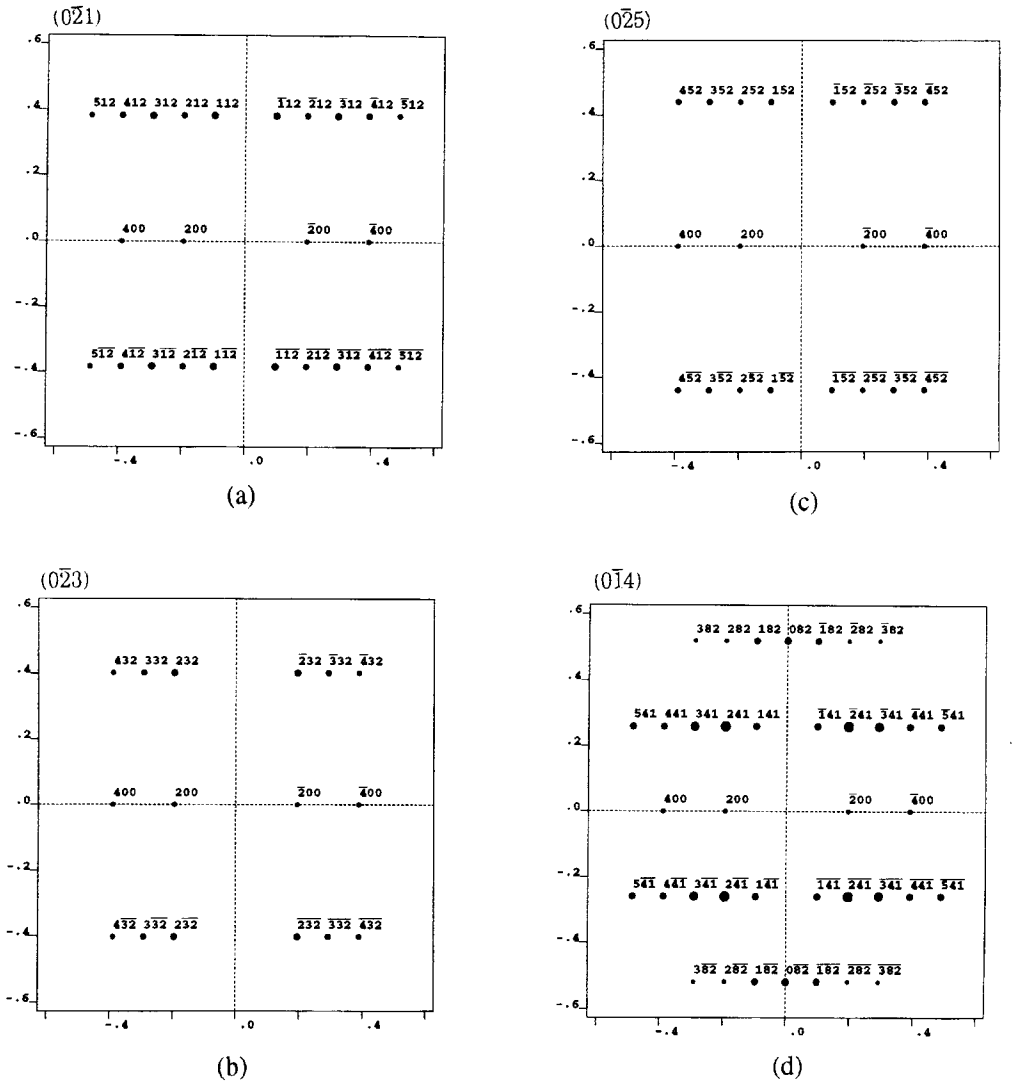

Fig. 9 Simulated electron diffraction patterns for tilt about a*

The absorption spectrum of 4-DMA-3-CB in methylcyclohexane is shown in Fig. 2. It shows at least three electronic transitions. Detailed information about the orientation of the transition dipole and the ground and excited state dipole associated with each transition can be obtained by electrooptical absorption measurements [8, 45, 46]. The quantitative results of these measurements carried out for 4-DMA-3-CB in methycyclohexane will be published later. For the weak band at ~ 350 nm the transition dipole is nearly parallel to the ground state dipole. It may give rise to small contributions to tensor components other than the dominant one, which are too weak to be resolved by the HRS-depolarization. For the intense second band at ~ 290 nm we found that the transition dipole is oriented nearly perpendicular to the ground state dipole and the change of the dipole during excitation. From an expression for β obtained by perturbation theory one can expect the second band to be dominant due to resonance enhancement and high integral absorption. In this case a tensorial two state model predicts a vectorial β-contribution aligned roughly perpendicular to the ground state dipole, which is in good agreement with the results described above.

Optical properties of crystals

In the light microscope both small and large crystals with different morphologies were observed. The second-harmonic-generation image in Fig. 3 was obtained at a

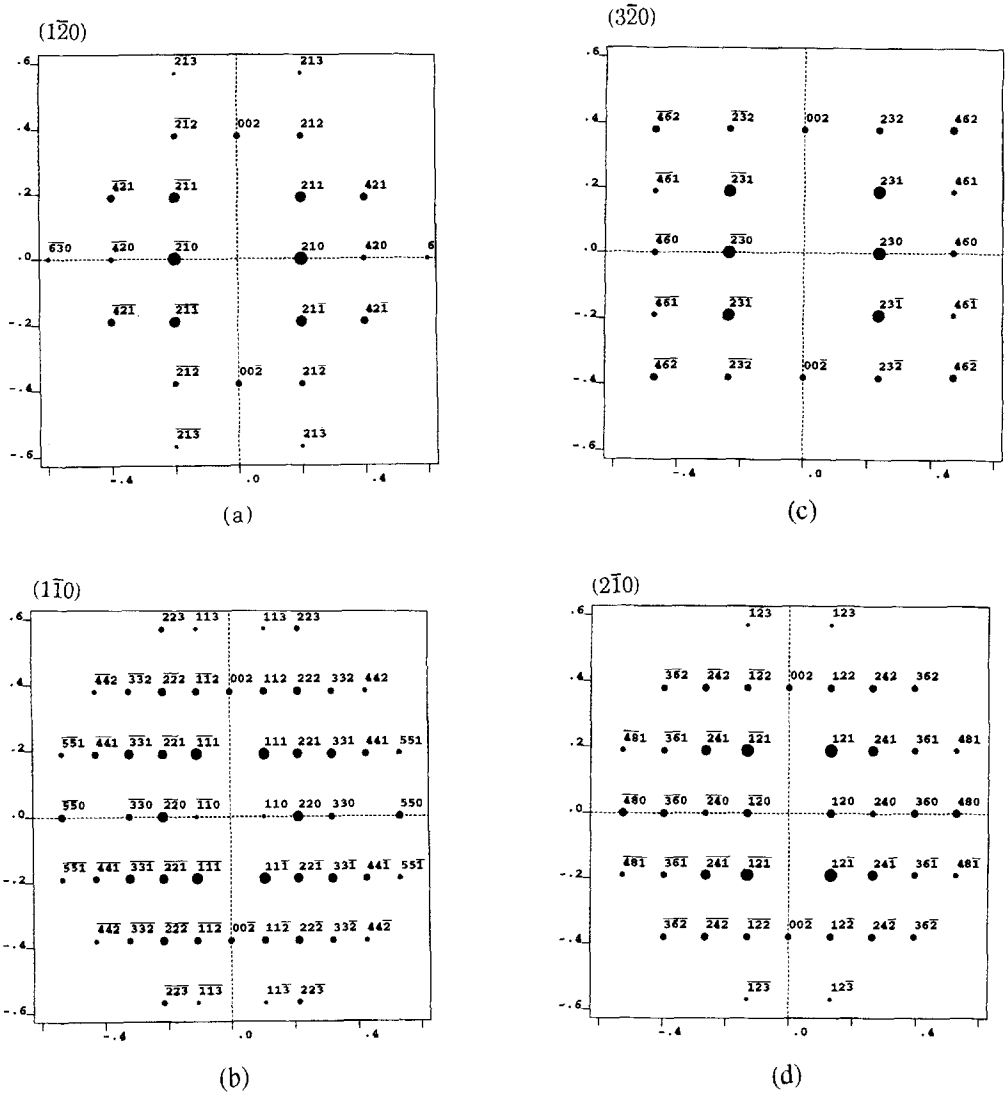

Fig. 10 Simulated electron diffraction patterns for tilt about c*

specific orientation of the small crystals using a camera attached to the Olympus microscope (STM 5-MJS) in place of a detector. The crystal in Fig. 3 was additionally illuminated in dark field geometry while exposed to the fundamental laser beam. The green spot in the middle shows the frequency doubled light where the Nd:YLF laser hits the sample. The signal is easily recognized with the naked eye. The maximum effect was observed when the polarization of the fundamental laser beam was perpendicular to the long axis of the crystal. Therefore the small crystals must be non-centro-symmetric.

The large crystals did not produce any SHG. Therefore the large crystals may be centro-symmetric or close to it.

Electron diffraction

A low resolution micrograph of the small crystals suitable for electron microscopy is shown in Fig. 4(a) together with the corresponding diffraction pattern Fig. 4(b). We have assigned the **a*** and **c*** axes as indicated in the diagram.

In Figs. 5(a)–(h) the crystal is tilted about the **a***-axis. New zones appear at $\pm 6°$, $\pm 12°$, $\pm 18°$, $\pm 24°$, $\pm 30°$, $\pm 34°$, $\pm 41°$ and $\pm 48°$. Subsequently, the crystal was rotated so that the **c***-axis was horizontal. Fig. 6(a)–(f) show tilts of 12, 18°, 24°, 31°, 35° and 42° about this axis. In both cases the diffraction patterns obtained by $\pm$-tilts were identical.

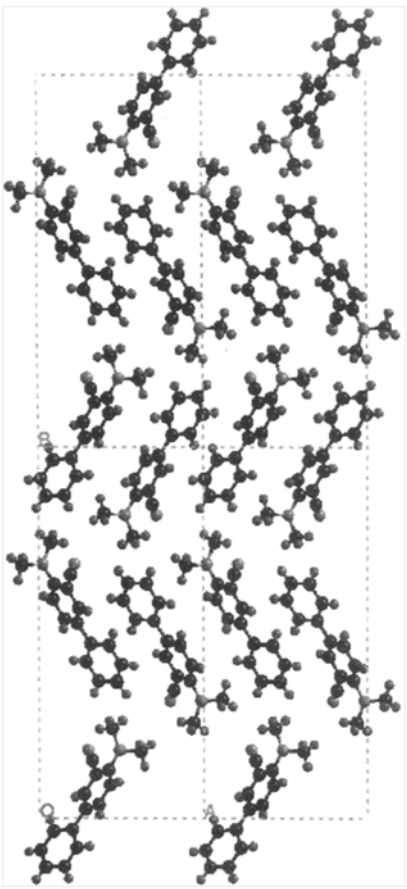

Fig. 11 Representation of ab projection in Pna21 crystal showing six unit cells to obtain over impression of molecular arrangement

Table 5 Atomic co-ordinates of small DMA-3CB Crystals in Pna21 space group with 4 molecules/unit cell. CELL 0.00 10.27 22.64 5.2700 90.00 90.00 90.00; LATT-1; SYMM-X, −Y, +Z + 0.500; SYMM + X + 0.500, −Y + 0.500, + Z; SYMM-X + 0.500, + Y + 0.500, +Z + 0.500

C1	0.73451	0.93821	0.71669
C2	0.66739	0.88341	0.73154
C3	0.58085	0.87332	0.91671
C4	0.56355	0.91914	1.09524
C5	0.63466	0.96993	1.08508
C6	0.72104	0.98334	0.89689
N7	0.51343	0.82119	0.95728
C8	0.37662	0.82579	1.03803
C9	0.56614	0.76222	0.95242
C10	0.70041	0.84458	0.53539
N11	0.73352	0.81355	0.36566
H12	0.79027	0.94444	0.58021
H13	0.50203	0.91456	1.22320
H14	0.62356	0.99727	1.21500
H15	0.56258	0.74573	1.11801
H16	0.51655	0.73851	0.83940
H17	0.65404	0.76355	0.89663
H18	0.34048	0.86158	0.97562
H19	0.32882	0.79325	0.97248
H20	037225	0.82547	1.21809
C21	0.79885	1.03670	0.89637
C22	0.92526	1.03810	0.78615
C23	0.99685	1.08972	0.79493
C24	0.95331	1.13958	0.91017
C25	0.82674	1.14089	1.01520
C26	0.75450	1.08908	1.00858
H27	1.00654	1.17272	0.91996
H28	1.07845	1.09033	0.71849
H29	0.95939	1.00458	0.70888
H30	0.67228	1.08916	1.08256
H31	0.79306	1.17525	1.08625

The tilt series about **a*** show the disappearance of a layer line in successive zones and the extinction of some reflections to be specified below.

The tilt series about **c*** confirms the presence of all (hkl) reflections in the 15 zones obtained experimentally.

Summarizing the results, the extinctions are as follows:

$h00: h = 2n$; $001: 1 = 2n$; $h01: h = 2n$;

$0kl: k + 1 = 2n$; hkl: no conditions .

Furthermore, the major axes remain perpendicular to one another throughout the tilting series and intensities symmetrical with respect to these axes, indicating an orthorhombic unit cell.

The International Tables show that the only orthorhombic space group consistent with these extinctions is the non-centrosymmetric $Pna2_1$ with 4 molecules per unit cell in equivalent positions.

x, y, z; $\bar{x}, \bar{y}, \frac{1}{2} + z$;

$\frac{1}{2} - x, \frac{1}{2} + y, \frac{1}{2} + z$; $\frac{1}{2} + x, \frac{1}{2} - y, z$.

Molecular conformation in gas phase

The MOPAC-calculated minimum energy molecular conformation closest to the conformation required in the crystal cell indicates the rotation of the two rings with respect to one another, as well as a rotation of the end group. The calculated value of μ is in excellent agreement with the experimental value obtained by permittivity measurements. The values of β have already been discussed earlier. In Fig. 7 the molecular rotations are indicated with respect to the central aromatic ring containing the acceptor C≡N group. The outer aromatic ring is rotated by $-47.56°$ w.r.t to this central core while the donor $N(CH_3)_2$ group is rotated by $+31.2°$ w.r.t the central core. This gives rise to a resultant dipole of $14.54 \cdot 10^{-30}$ Cm and a resultant second order polarizability of $-0.49 \cdot 10^{-50}\ Cm^2V^{-2}$ in the direction along the dipole. The details about the individual components contributing to these values are given in the Tables 3 and 4. It is seen that the major component of β is virtually along the

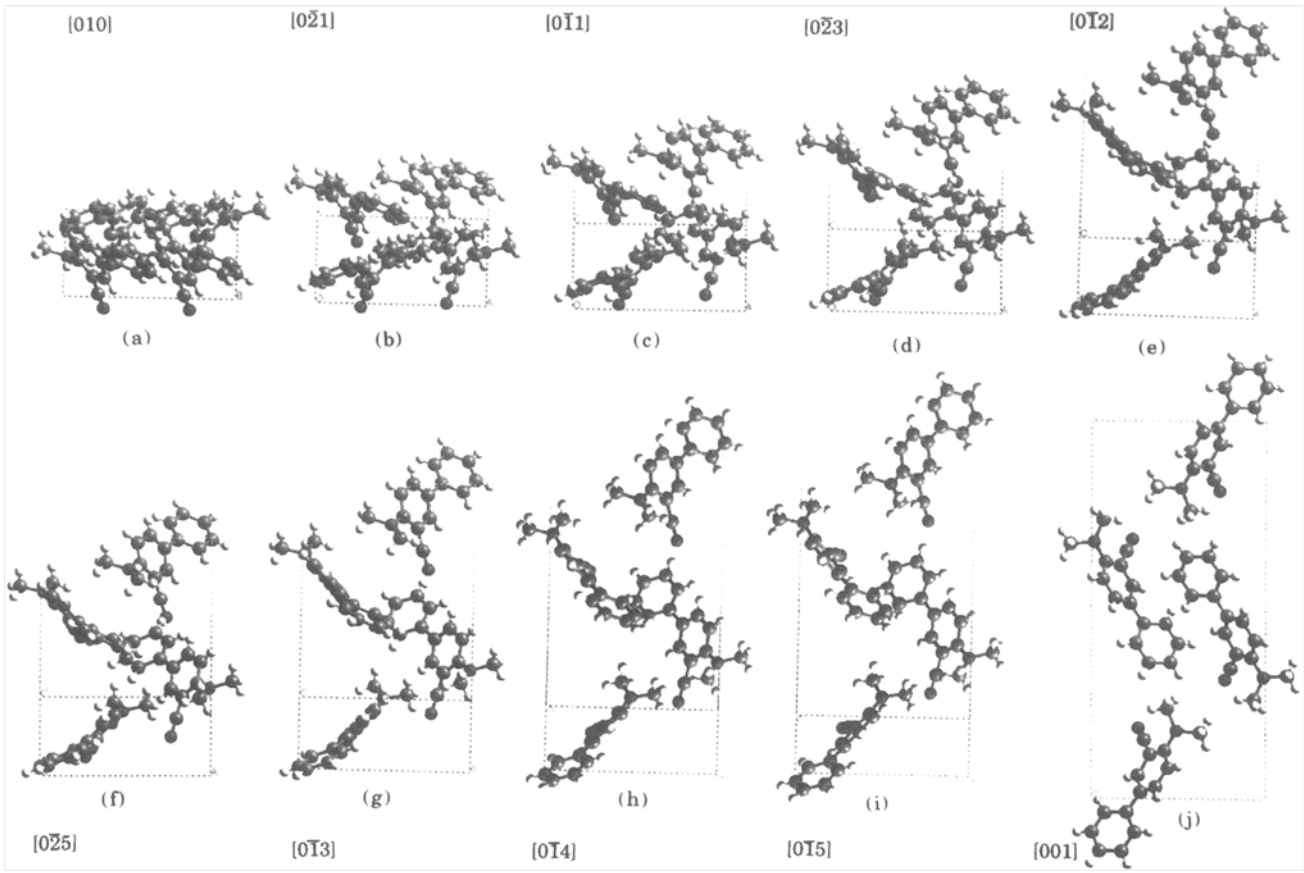

Fig. 12 Representation of major projections in $Pna2_1$ crystal corresponding to zones indicated in brachets

molecular axis, while the dipole μ is almost perpendicular to it, exactly corroborating the HRS and EFISH result.

Simulation of electron diffraction patterns

Extremely good qualitative agreement between the experimental and simulated electron diffraction patterns was obtained in all 15 zones for the molecular conformation and packing indicated in Fig. 8, which also shows the relationship between the unit cell and the macroscopic single crystals.

Figures 9(a)–(h) and 10(a)–(f) show the simulated diffraction patterns for all the zones obtained experimentally and clearly demonstrate the good qualitative agreement with Figs. 4–6. The unit cell and space group used for these simulations has the following dimensions:

$a = 10.28$ Å; $b = 22.64$ Å;

$c = 5.27$ Å; $\alpha = \beta = \gamma = 90°$.

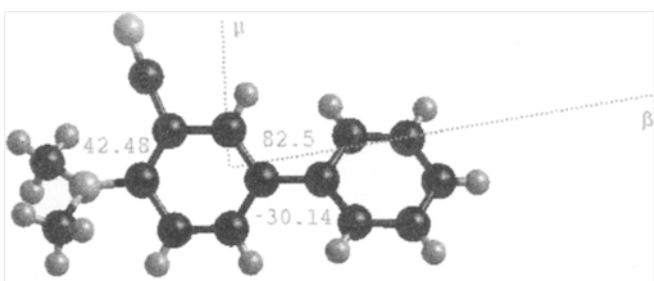

Fig. 13 Molecular conformation in crystal

There are four molecules/unit cell in space group $Pna2_1$. Refinement of intensities in all zones finally led to a negative packing energy of -84 kcal/mol. After removal of all non-allowed bond distances, the molecular conformation and orientation indicated in Fig. 11 is obtained. The atomic coordinates are given in Table 5. Other projections corresponding to the diffraction zones indicated in

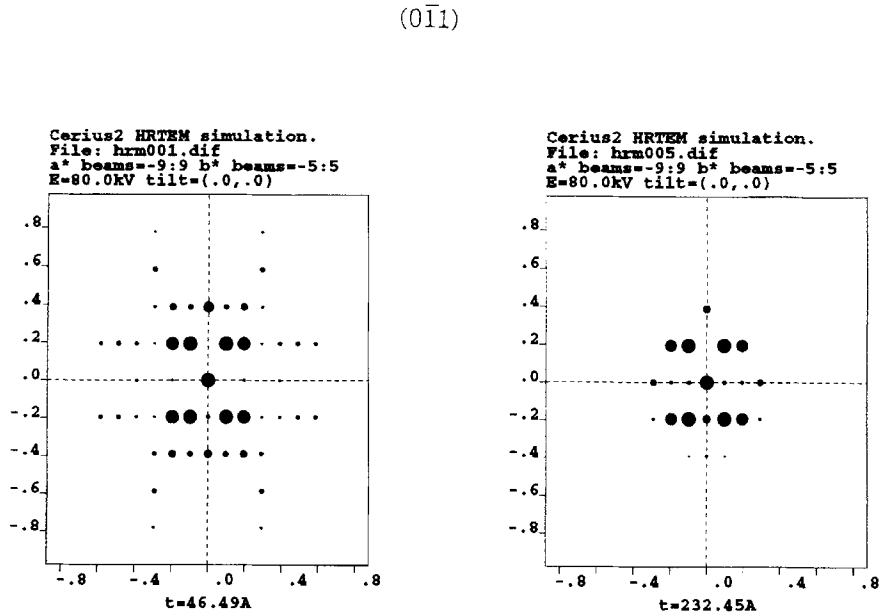

Fig. 14 Effect of dynamica scattering on (0 $\bar{1}$ 1) zone as a function of sample thickness

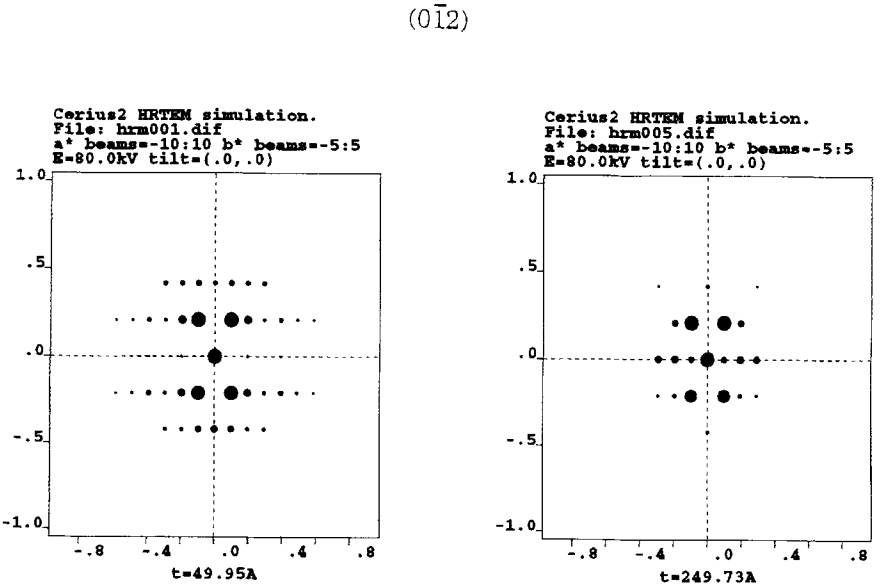

Fig. 15 Effect of dynamica scattering on (0 $\bar{1}$ 2) zone as a function of sample thickness

brackets are shown in Fig. 12(a)–(h). From these simulations it is apparent that the most favorable projection for imaging would be the ab projection corresponding to the [0 0 1] diffraction zone. This zone is, in fact, not accessible since it would require viewing down the side of flat platelets. In the most easily available ac projection, the molecules project upwards towards the observer at different angles and thus overlap in projection. Since we have solved an unknown structure, the atomic coordinates are given in Table 5.

The molecular conformation corresponding to this structure is shown in Fig. 13. Due to the crystal field, the molecular rotation with respect to the central core is slightly adjusted. The aromatic ring is now rotated by $-30.14°$ and the $N(CH_3)_2$ group by 48.84°. The dummy atoms indicate how the directions of μ and β are affected. The largest component of μ is $11.71 \cdot 10^{-30}$ Cm in the molecular y direction and β is $5.39 \cdot 10^{-50}$ Cm^3V^{-2} in the molecular x direction along the long axis of the molecule. Details are listed in Table 4. Unfortunately, these major components of β of four molecules oppose each other in the unit cell (see Fig. 12(j)) while only the smaller in the z-direction re-enforce each other. The resultant components of μ for all four molecules are shown in Table 4.

Fig. 16 Effect of dynamical scattering on (0 $\bar{1}$ 3) zone as a function of sample thickness

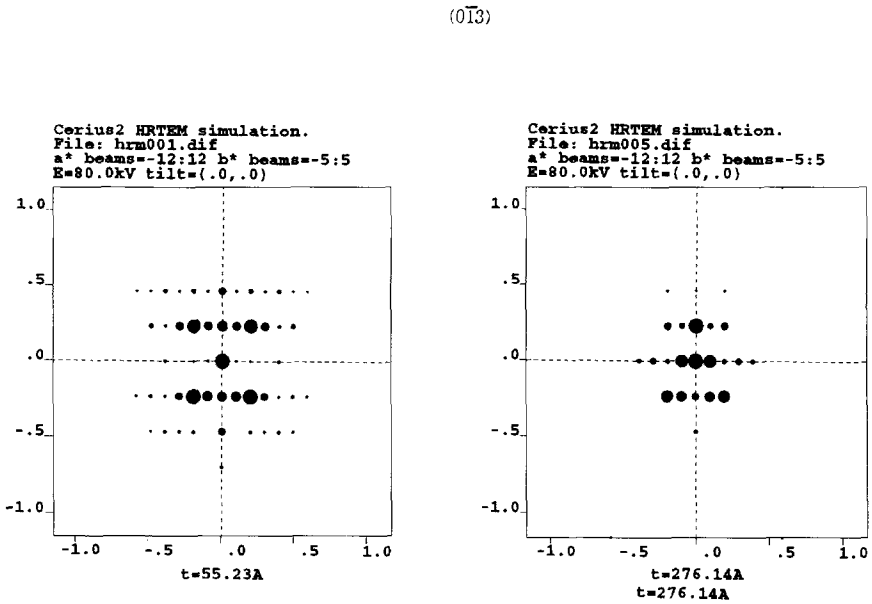

The largest component of $38.99 \cdot 10^{-30}$ Cm is along the crystallographic c direction.

Calculation of the second order polarizability tensor in unit cell

The resultant second order polarizability with respect to the crystal axes was calculated as follows:

The crystal cell consisting of four 4-DMA-3CB molecules, as determined by electron diffraction crystal structure analysis, was treated as one supermolecule for MOPAC second order polarizability calculations. It is necessary to calculate the second order polarizability tensor and its vector components in the coordinate system related to the unit cell of the crystal structure, i.e. *a*, *b*, and *c* crystal axes should be parallel to *x*, *y*, and *z* axes of cartesien coordinate system respectively. It should be noted that usually the MOPAC program changes the orientation of a molecule along one of the axes of the cartesian coordinate system [16]. In order to prevent this, four dummy atoms were added to the MOPAC input file containing cartesian coordinates of the atoms of the supermolecule in the orthorhombic unit cell of 4-DMA-3CB. These four dummy atoms had the numbers 1, 2, 3, 4 and were placed in the origin, on *x* axis, on *y* axis and on *z* axis, respectively. Thus, it was possible to calculate second order polarizability tensor and its vector components in the cartesian coordinate system directly related to the crystallographic axes (Table 4). This component of $4.22 \cdot 10^{-50}$ Cm^3V^{-2}/unit cell in the *c* direction gives the major contribution towards the total β of $433 \cdot 10^{-50}$ Cm^3V^{-2}/unit cell and is responsible for the observation of green light in the NLO experiment.

Dynamical scattering

In order to ascertain whether the structure determination was seriously affected by dynamic scattering, the intensity distribution in different zones was calculated as a function of thickness *t*, using the multislice methods incorporated in CERIUS [19, 20]. Figures 14–16 show the results for the [0 $\bar{1}$ 1], [0 $\bar{1}$ 2], [0 $\bar{1}$ 3] zones. As we have shown on previous occasions, the individual intensities are already affected by dynamical scattering at 100 Å [22, 25, 32] and major changes in intensity distribution become evident at 150 Å, therefore the sample thickness was kept below this value.

X-ray methods

X-ray powder pattern

A powder x-ray diffraction pattern was obtained in order to ascertain 1) whether symmetry-forbidden reflections due to dynamical scattering have arisen in the electron diffraction patterns, 2) In order to improve the *d*-values obtained by electron diffraction and 3) to test the model.

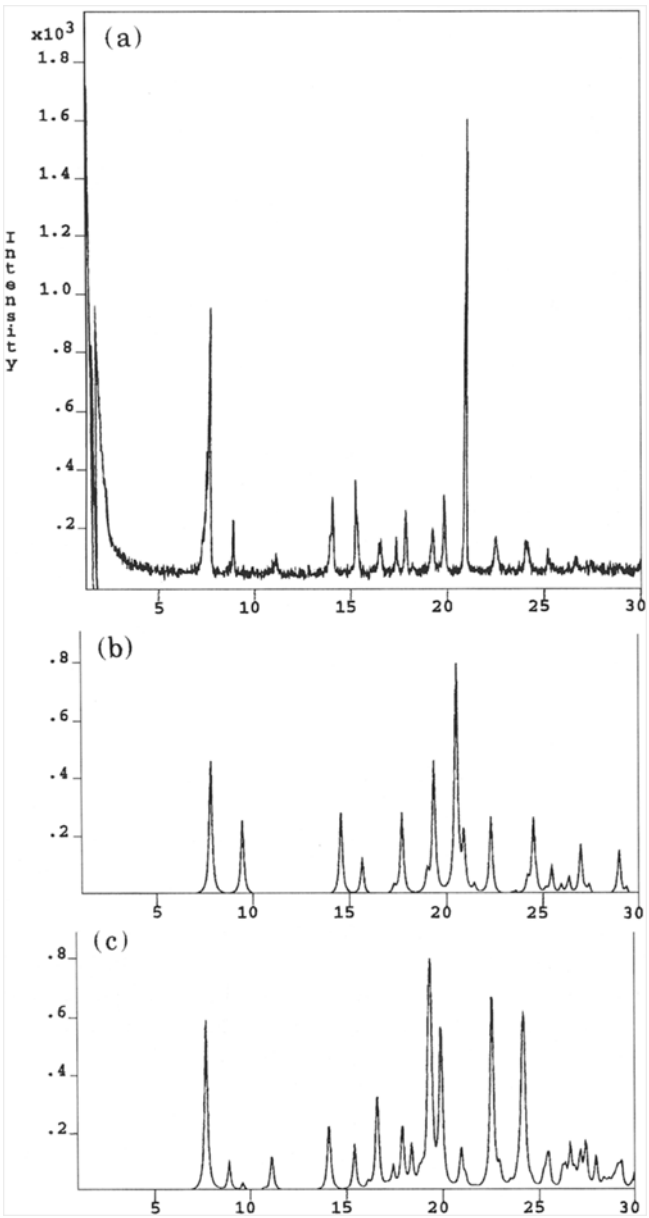

Fig. 17 Comparison between experimental x-ray powder pattern (a) and calculated x-ray powder pattern from models obtained by electron diffraction (b) and x-ray analysis (c)

The experimental diffraction pattern is shown in Fig. 17(a). In Fig. 17(b), the calculated powder x-ray pattern for the model obtained from the electron diffraction analysis is shown. It can be seen that the experimental x-ray powder pattern contains additional maxima. The explanation for this phenomenon lies in the presence of additional crystals with a different crystal structure, as will be shown in the following section.

Table 6

Crystal data for VOIGT4	
formular	$C_{15}H_{14}N_2$
weight	222.3 $gmol^{-1}$
crystal size	$0.16 \times 0.192 \times 0.704$ mm
absorption	$\mu = 0.55$ mm^{-1} no absorptions correction
space group	P1 triclinic
lattice parameters	$a = 9.782(7)$ Å $\alpha = 86.65(1)°$
(calculated from	$b = 11.434(2)$ Å $\beta = 78.10(2)°$
16 reflections with	$c = 23.440(6)$ Å $\gamma = 73.71(6)°$
$37° < \Theta < 43°$)	$V = 2462(2)$ $Å^3$ $z = 8$ F(000) = 944
temperature	295 K
density	$d_x = 1.199$ gcm^{-3}
Data collection	
diffractometer	CAD4 (Enraf-Nonius)
radiation	Cu-K_α graphite monochromator
scan-type	$\omega/2\Theta$
scan-width	$0.7 + 0.14 * \tan(\Theta)$ and 25% left and right for background determination
scan range	$1.5° \leq \Theta \leq 70.0°$ $-11 \leq h \leq 11$ $-13 \leq k \leq 13$ $-26 \leq 1 \leq 26$
Nr. of reflections:	
measured	11777
unique	11777
observed	4125 ($\|F\|/\sigma(F) > 4.0$)
Data correction, structure solution and refinement	
corrections	Lorentz- and polarization correction, decay of intensity (10%) corrected with cubic spline function.
solution	program: SIR-92 (direct methods)
refinement	program- SHELXL93 (full matrix refinement) 1226 refined parameters, weighting schema: $w = 1/\|\sigma^2(F_0) + (0.249 * P)^2\|$: with $P = (\text{Max}(F_0^2, 0) + 2 * F_c^2)/3.0$ H-atoms at geometric calculated positions, refined with riding motion. Non H-atoms anisotropic refined.
R-values	$wR_2 = 0.4468$ ($R_1 = 0.1122$ for observed reflections with $F_0 > 4\sigma(F_0)$)
goodness of fit	$S = 0.992$
maximal deviation of parameters	0.005 * e.s.d
maximal peak height in diff. Fourier map	0.33, -0.32 $eÅ^{-3}$

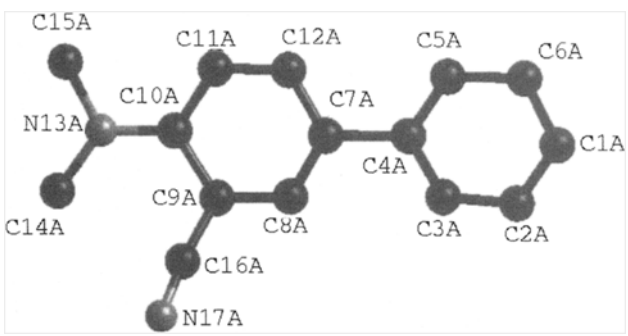

Fig. 18 Molecular labeling on atoms related to atomic positions in Table 4

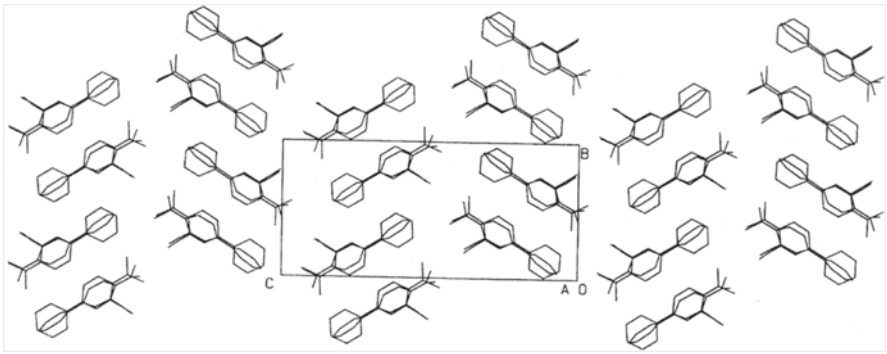

Fig. 19 Representation of bc projection of P1 crystal

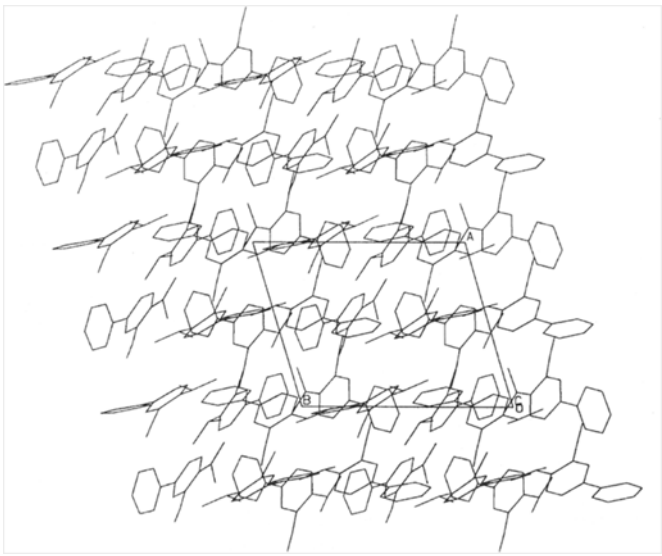

Fig. 20 Representation of ab projection of P1 Crystal

X-ray analysis and refinement

The NLO experiment had already indicated the presence of two kinds of crystals: a) small crystals suitable for electron diffraction showing second harmonic generation and b) large crystals suitable for x-ray analysis but without second harmonic generation. The results of the x-ray structure analysis and refinement using the labeling indicated in Fig. 18 are listed in Table 6. The unit cell is triclinic, space group P1, almost $P\bar{1}$, cell constants are indicated below:

$a = 9.782(7)$ Å $\quad \alpha = 86.65(1)^\circ$

$b = 11.434(2)$ Å $\quad \beta = 78.10(2)^\circ$

$c = 23.440(6)$ Å $\quad \gamma = 73.71(6)^\circ$.

There are eight molecules/unit cell. They are arranged as indicated in Figs. 19–21 looking down the *a*, *c* and *b* axes, respectively. Especially in the projection down *a*, it is clear that pairs of molecules are arranged almost centro-symmetrically. The molecular conformation and arrangement in pairs is analyzed in detail in Fig. 22. Due to the fact that the arrangement of the molecules in the unit cell is almost centro-symmetric, the large crystals do not cause second harmonic generation.

The calculated x-ray powder pattern from this structure is shown in Fig. 17(c). It can be seen that the additional reflections in the experimental powder pattern are now evident.

It is clear that the experimental powder pattern contains reflections from both types of crystal.

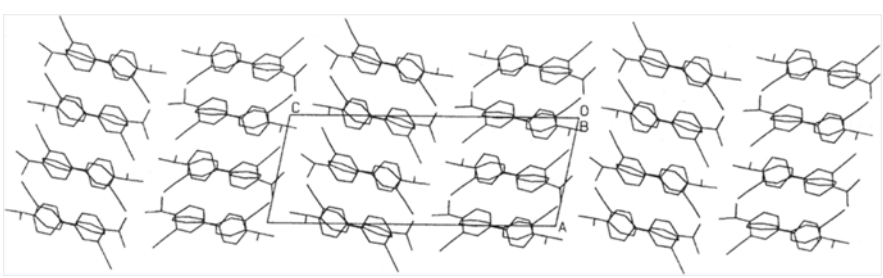

Fig. 21 Representation of ac projection of P1 crystal

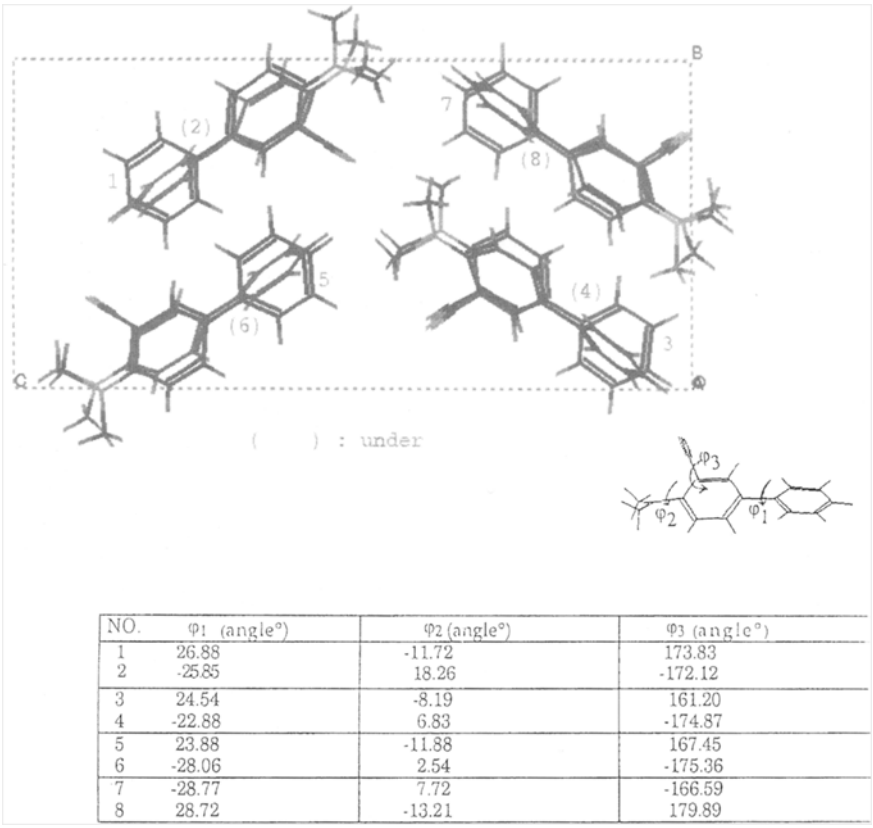

NO.	φ1 (angle°)	φ2 (angle°)	φ3 (angle°)
1	26.88	-11.72	173.83
2	-25.85	18.26	-172.12
3	24.54	-8.19	161.20
4	-22.88	6.83	-174.87
5	23.88	-11.88	167.45
6	-28.06	2.54	-175.36
7	-28.77	7.72	-166.59
8	28.72	-13.21	179.89

Fig. 22 Molecular conformations of the eight molecules in the unit cell of the P1 crystals, indicating values of torsional angles ϕ_1, ϕ_2, ϕ_3

Conclusion

We have shown that a thorough understanding of the molecular properties can be achieved only by combining different fields of expertise.

The non-linear properties of organic molecules and crystals have been discussed in many standard and specialized text books [16, 47]. In particular, the structural dependence of non-linear optical properties of organic molecules has been studied in detail by Zyss in several articles of which one, in particular, provides a thorough basic understanding of the relationship between the non-linear susceptibility tensor of single crystals and the second order polarizability tensors of the constituent molecules, using x-ray structural data [47].

In this work we have shown that the required structural data can now be obtained from electron diffraction data as well. This development is important for the following reasons:

1) Many organic crystals are too small for x-ray analysis.

2) In many solvents different crystals are obtained, depending on temperature and cooling rate. It is possible that as in this case, the smaller, non-equilibrium crystals obtained from at large undercooling are those giving the desired non-centrosymmetric structure.

For 4-DMA-3-CB we determined the dipole and the second order polarizability tensor β in solution. The latter was studied by a combination of polarization dependent EFISH- and HRS-measurements and found to be dominated by one single component giving rise to a vector part roughly perpendicular to the dipole. This fits well with the results of the PM3-calculations and permitted a deeper insight into the NLO-properties in the crystalline state.

For the NLO-active crystals, the major components of the second order polarizability parallel to the long molecular axis unfortunately virtually cancel. However, the other components are still large enough to give rise to an effect which can be observed with the naked eye.

Acknowledgment Financial support of the Deutsche Forschungsgemeinschaft, the Volkswagen-Stiftung and the Fonds der Chemischen Industrie is gratefully acknowledged.

References

1. Willets A, Rice JE, Burland DM, Shelton DP (1992) J Chem Phys 97:4590
2. Terhune RW, Maker PD, Savage CM (1965) Phys Rev Letters 66:681
3. Clays K, Persoons A (1991) Phys Rev Lett 66:2980
4. Clays K, Persoons A (1992) Rev Sci Instrum 63:3258
5. Zyss J, Van TC, Dhenaut C, Ledoux I (1993) Chem Phys 177:281
6. Wolff JJ, Längle D, Hillenbrand D, Wortmann R, Matschiner R, Glania C, Krämer P, Adv Mater, in press
7. Liptay W, Wehning D, Becker J, Rehm T, Naturforsch Z (1982) 37a:1369
8. Wortmann R, Elich K, Lebus S, Liptay W, Borowicz P, Grabowska A (1992) J Phys Chem 96:9724
9. Heesink GJT, Ruiter AGT, van Hulst NF, Bölger B (1993) Phys Rev Lett 71:999
10. Andrews DL (1994) Adv Chem Phys 85:545
11. Verbiest T, Clays K, Samyn C, Wolff JJ, Reinhoudt D, Persoons A (1994) J Am Chem Soc 116:9320
12. Hendrickx E, Clays K, Persoons A, Dehu C, Brédas JL (1995) Am Chem Soc 117:3547
13. Andrews DL, Thirunamachandran T (1977) J Chem Phys 67:5026
14. Levine BF, Bethea CG (1975) J Chem Phys 63:2666
15. Wortmann R, Krämer P, Glania C, Lebus S, Detzer N (1993) Chem Phys 173:99, 229:101 (1994)
16. Nye JF (198) Physical properties of crystals
17. Kurtz H, Stewart J, Dieter K (1990) J Comput Chem 11:82
18. Clays K, Persoons A, de Maeyer L (1994) Adv Chem Phys 85:455
19. Cowley J (1988) Diffraction physics. North Holland
20. Cowley J (1992) Electron Diffraction Techniques, Vol. 1 Ed. Oxford Science Publications
21. Dorset D (1985) J Electron Microscopy Technique 2:89
22. Voigt-Martin IG, Yan DH, Gilmore C, Shankland K (1994) Ultramicroscopy 56:271
23. Voigt-Martin I, Schumacher M, Garbella R (1992) Macromolecules 25:961
24. Voigt-Martin IG, Simon P, Yan DH, Yakimaski A, Bauer S, Ringsdorf H (1995) Macromolecules 28:243
25. Voigt-Martin IG, Yan DH, Wortmann R, Elich K (1995) Ultramicroscopy 57: 29–43
26. Lequan M, Branger C, Simon J, Thami T, Chauchard E, Persoons A, Chem Phys Lett
27. Loos-Wildenauer M, Kunz S, Yakimanski A, Voigt-Martin IG, Wischerhoff E, Zentel R, Tschershe C, Müller M (1995) Advanced Materials, 7(2): 170–174
28. Crewe A, Isaacson MS, Zeitler E (1976) In: Hoppe W, Mason R, ed. Advances in Structure Research. Vol. 7 Pergamon, New York
29. Henderson R, Glaeser R (1985) Ultramicroscopy 16:28
30. Voigt-Martin I, Durst H (1987) Liquid Crystals 2:585
31. Voigt-Martin IG, Garbella R, Schumacher M (1994) Liquid Crystals 17: 775 801
32. Voigt-Martin IG, Yan DH, Yakimanski A, Schollmayer D, Gilmore CJ, Bricogne G (1995) Acta Cryst A51:849–868
33. Dorest D (1990) EMSA Bulletin 20:1 54–63
34. Dorset D (1991) Acta Cryst A 47:510
35. Dong W, Baird T, Fryer JR, Gilmore CJ, MacNicol DD, Bricogne G, Smith DJ, Keefe MAO, Hovmöller S (1992) Nature (Lond) 355:605
36. Gilmore CJ, Shankland K, Fryer JR (1993) Ultramicroscopy 49:132–146
37. Sheldrick GM, SHELX-86: Program for the solution of crystal structures. Univ. of Göttingen, Germany
38. Sheldrick GM, SHELX 93, Program for crystal structure determination, Univ. Cambridge, England
39. Bingham R, Dewar MS, Lo DH (1975) J Amer Chem Soc 97:1285–1295
40. Stewart JP (1989) Journal of Computational Chemistry 10:209–220
41. Mayo S, Olafson B, Goddard WA (1990) J Phys Chem 94:8897
42. Karasawa N, Goddard WA (1989) J Phys Chem 93:7320
43. Ledoux I, Zyss J, Jutant A, Amatore C (1991) Chem Phys 150:117
44. Zyss J, Ledoux I, Bertault M, Toupet E (1991) Chem Phys 150:125
45. Liptay W, In: Lim EC, Excited States, Vol. 1. Dipole moments and polarizabilities of molecules in excited electronic states, ed. (Academic Press, New York, 1974) p 129
46 Liptay W, Wortmann R, Schaffrin H, Burkhard O, Reitinger W, Detzer N (1988) Chem Phys 120:429
47. Chemla DS, Zyss J (1987) Non-linear optical properties of organic molecules and crystals. Vol. I, II ed., Academic Press